Pharm Res (2013) 30:1799–1812
DOI 10.1007/s11095-013-1024-5

RESEARCH PAPER

Riboflavin-Targeted Polymer Conjugates for Breast Tumor Delivery

Lisa M. Bareford • Brittany R. Avaritt • Hamidreza Ghandehari • Anjan Nan • Peter W. Swaan

Received: 10 January 2013 / Accepted: 4 March 2013 / Published online: 9 April 2013

ABSTRACT

Purpose In breast cancer, a significant decrease in riboflavin (RF) serum levels and increase in RF carrier protein occurs, indicating a potential role of RF in disease progression. To evaluate RF's ability to serve as a targeting agent, mitomycin C (MMC)-conjugated N-(2-hydroxypropyl)methacrylamide (HPMA) copolymers were synthesized and targeted to the RF internalization pathway in human breast cancer cells.

Methods Competitive uptake studies were used to determine specificity of RF-targeted conjugates, and an MTT assay established the IC_{50} for the conjugates. Endocytic mechanisms were investigated by confocal microscopy.

Results Studies revealed a high-affinity endocytic mechanism for RF-specific internalization of fluorescently-labeled conjugates in both MCF-7 and SKBR-3 cells, whereas folic acid-mediated endocytosis showed high specificity only in SKBR-3 cells. MMC internalization was significantly higher following nontargeted and RF-targeted MMC-conjugate administration compared to that of free MMC. Cytotoxic analysis illustrated potent IC_{50} values for RF-targeted MMC conjugates similar to free MMC. Maximum nuclear accumulation of MMC resulted from lysosomal release from RF-targeted and nontargeted MMC-conjugates following 6 h incubations, unlike that of free MMC seen within 10 min.

Conclusion Targeting polymer-MMC conjugates to the RF internalization pathway in breast cancer cells enabled an increase in MMC uptake and nuclear localization, resulting in potent cytotoxic activity.

KEY WORDS breast cancer · nanomedicine · receptor-mediated endocytosis · riboflavin · targeted delivery

ABBREVIATIONS

DIPEA	Diisopropyl ethylamine
DMEM	Dulbecco's modified eagle medium
DMF	Dimethylformamide
DMSO	Dimethyl sulfoxide
DPBS	Dulbecco's phosphate buffered saline
EDTA	Ethylenediaminetetraacetic acid
FA	Folic acid
FITC	Fluorescein isothiocyanate
HBSS	Hank's balanced salt solution
HPMA	N-(2-hydroxypropyl)methacrylamide
LAMP-1	Lysosomal-associated membrane protein 1
MMC	Mitomycin C
MTT	3-(4,5-dimethylthiazol-2-yl)-2,5-diphenyltetrazolium bromide
RCP	Riboflavin carrier protein
RF	Riboflavin
RME	Receptor-mediated endocytosis
TFA	Trifluoroacetic acid
THF	Tetrahydrofuran

INTRODUCTION

Chemotherapeutic agents lack drug specificity at the tumor site, thereby significantly limiting their therapeutic utility. To control the indiscriminate diffusion of anticancer drug molecules, macromolecular vehicles have been extensively investigated as

L. M. Bareford · B. R. Avaritt · H. Ghandehari · A. Nan · P. W. Swaan (✉)
Department of Pharmaceutical Sciences
Center for Nanomedicine and Cellular Drug Delivery
University of Maryland Baltimore
20 Penn Street, Health Sciences Facility 2, Room 543
Baltimore, Maryland 21201, USA
e-mail: pswaan@rx.umaryland.edu

Present Address:
H. Ghandehari
Department of Pharmaceutics & Pharmaceutical Chemistry
& of Bioengineering, Utah Center for Nanomedicine, Nano Institute of Utah, University of Utah, Salt Lake City, Utah 84108, USA

an alternative delivery strategy. Conjugating chemotherapeutics to biocompatible carriers offers many advantages including enhanced drug solubility, increased tumor accumulation, and reduced toxicity (1,2). Being primarily limited to endocytic internalization, nanoscale drug conjugates are retained in blood circulation longer, enabling passive accumulation in tumor tissue by means of the enhanced permeability and retention (EPR) effect (3) or by active targeting using receptor-mediated endocytosis (RME). In addition, vesicular internalization may potentially avoid cellular drug-resistance mechanisms, such as efflux transporters, to permit higher cytosolic drug concentrations (4). Ligand-targeted therapeutics take advantage of their intracellular localization to the acidic and enzyme-rich endolysosomal compartments through biodegradable spacers which are pH (5) and enzyme (6) sensitive.

Cell-surface vitamin-B receptors facilitate the efficient absorption of nutrients that are essential for normal cellular growth and metabolism, but particularly important for the exponential development of tumor cells (7). High-affinity RME facilitates the efficient absorption of B-vitamins following dietary intake (8) and certain vitamin receptors are significantly upregulated in cancer cells (7,9), allowing for possible tumor-specific delivery of chemotherapeutics (10). However, the extent of vitamin receptor overexpression and ligand-selectivity varies by cancer type (11). For example, the folate receptor (FRα) is overexpressed in over one-third of human cancers (12) including 90% of ovarian cancers, but less than 25% of the various breast cancer forms (13). Overall, considerable evidence supports the therapeutic utility of vitamin-targeted drug conjugates.

Breast cancer remains the highest cause of malignancy-related death for women in the United States (14). A specific plasma protein marker for breast cancer, riboflavin carrier protein (RCP), was identified following clinical studies that revealed elevation in RCP serum levels (15) with simultaneous decrease in RF levels (16) in breast cancer patients. This effect is suggested to be the result of an upregulation in RF-specific cell surface receptors and RF internalization similar to other vitamin systems (7). While studies of avian-RCP suggest the protein aids in the recruitment of RF to a RF-specific plasma membrane associated receptor (17), the sequence of the human ortholog of RCP has yet to be elucidated, and no RF receptor has been identified. Kinetic analysis of RF internalization was conducted in a variety of cell lines where all systems revealed a high-affinity, saturable mechanism that is Na^+-, potential-, and pH-independent, suggesting an RF-specific carrier-mediated system (18). Further characterization in human breast cancer cells demonstrated RF absorption to occur predominantly *via* RME at physiological concentrations (~ 12 nM) (19,20) prior to vesicular trafficking to subcellular organelles (21). This data suggests a clinical application for RF as a novel targeting agent for breast cancer-directed chemotherapeutics.

To utilize RF targeting the water-soluble polymer N-(2-hydroxypropyl)methacrylamide (HPMA) was employed as a biocompatible drug delivery vehicle due to its versatile synthetic chemistry (22–24). The highly effective breast cancer compound mitomycin C (MMC) was selected because of its significantly limited clinical utility (25). Both RF and folic acid (FA) were used as targeting ligands to examine the targeting potential of RF for the selective absorption of polymeric-MMC conjugates in two breast cancer cell models, MCF-7 and SKBR-3. The *in-vitro* efficacy of RF-targeted MMC-conjugates was characterized by evaluating cellular internalization, cytotoxicity, subcellular trafficking, and drug stability.

MATERIALS AND METHODS

Chemicals

MMC was purchased from Bristol Laboratories (Evansville, IN). Unless otherwise mentioned all other chemicals were reagent grade and obtained from Sigma (St. Louis, MO).

Synthesis of Comonomers and Polymers

Synthesis of Monomers

HPMA comonomer (26) and peptide containing comonomers N-methacryloyl-glycylphenylalanylleucylglycine *p*-nitrophenyl ester (MA-GFLG-ONp) (27), N-methacryloylglycylglycine *p*-nitrophenyl ester (MA-GG-ONp) (28), and 5-[3-(methacryloylaminopropyl)thioureidyl] fluorescein (MA-AP-FITC) (29), were synthesized according to well established procedures. Methacryloyl-GFLG-MMC (MA-GFLG-MMC): MA-GFLG-ONp was reacted with a reactive equivalent (eqv) of MMC in N,N-dimethylformamide (DMF) at 4°C, followed by the slow addition of an eqv of triethylamine. The mixture was then left to react in the dark for 4 h at RT. After overnight mixing at 4°C, the mixture was vacuum evaporated to remove DMF and the resulting purple-colored solid product, MA-GFLG-MMC, was extracted using diethyl ether precipitation.

Copolymerization

Experimental copolymers were synthesized by free radical precipitation copolymerization of monomer subunits using standardized reaction conditions (30). Fluorescently labeled polymer conjugates were prepared by copolymerization of HPMA (88 mol%), MA-GG-ONp (10 mol%), and MA-AP-FITC (2 mol%) comonomers. Experimental drug polymer conjugates were produced by copolymerization with HPMA (85 mol%), MA-GG-ONp (10 mol%), and MA-GFLG-MMC (5 mol%) comonomers. Control polymer conjugates

were prepared similarly, where MA-GFLG-ONp replaced the drug-containing monomer MA-GFLG-MMC. For each set of experimental conjugates, comonomers were solubilized in acetone-dimethyl sulfoxide (DMSO < 10% total volume) at 12.5 wt% with 1.2 wt% radical initiator (2,2'-azobisisobutyronitrile). Reaction mixtures were sealed under nitrogen in an ampoule and left to react at 50°C for 24 h. Precipitated polymers were dissolved in methanol and reprecipitated in acetone-ether to obtain the pure product.

Synthesis and Polymer Functionalization of Targeting Ligands

Synthesis of RF linker (RFl)

RF was amine-functionalized at its ribityl side chain to allow for stable conjugation to polymer-incorporated Gly-Gly dipeptide side chains. First, 10 mmol RF was reacted with 5 mmol succinic anhydride in DMSO including 5% (v/v) pyridine overnight at 80°C to promote monosubstitution at the primary hydroxyl position on the ribityl side chain of RF. The monosubstituted product was purified with a silica gel column using a methanol/chloroform gradient elution. Next, the resulting RF succinamide was reacted with an eqv of O-(N-succinimidyl)-N,N,N,N'-tetra-methyluronium tetrafluoroborate in DMF-dioxane solution containing 10% (v/v) water and diisopropyl ethylamine (DIPEA) for 45 min. To this mixture, 11 mmol of N-BOC-ethylenediamine in DMF was added and left to react for 4 h. The product was concentrated and purified using silica gel column chromatography using 5% MeOH in chloroform as the eluent. The resulting BOC-protected functionalized RF was concentrated, washed with acetone, and characterized (*m/z* 519 (MH^+), decomposition temperature 314–317°C).

Synthesis of FA linker (FAl)

Following methods standardized by Luo *et al.* (31), 4.5 mmol of folic acid was solubilized in tetrahydrofuran (THF), and an excess of trifluoroacetic acid (TFA) was added drop wise. The solution was stirred overnight at room temperature to obtain N10-(trifluoroacetyl)pyrofolic acid. The pyrofolic acid product was reacted with an eqv of N-BOC-ethylenediamine in DMF at 40°C overnight. Folate-ethylenediamine-BOC was then deprotected in neat TFA to yield folate-ethylenediamine which was precipitated in methanol to obtain the final FA-based targeting moiety (*m/z* 355 (MH^+), decomposition temperature 289–292°C).

Polymer Functionalization with Targeting Moieties

Experimental copolymers were functionalized by the addition of targeting ligand following RFl or FAl conjugation to polymer-incorporated reactive Gly-Gly spacers (Fig. 1). Fluorescently-labeled copolymers were prepared with either RF (P1-RF) or FA (P1-FA) targeting moieties. Copolymers both without (P2) and with (P3) drug were functionalized with two different amounts of the RF targeting moiety (P2B/C and P3B/C). Deprotected RFl or FAl were reacted overnight with copolymer conjugates in DMSO containing an eqv of DIPEA. Unreacted GG-ONp spacers were neutralized by 1-amino-2-propanol hydrolysis. The resulting RF- and FA-copolymers were dialyzed for 72 h in the dark to remove unconjugated targeting moieties and then used for further characterization. Neutral, nontargeted control copolymers were also prepared for each of the copolymer formulations (P1, P2A, and P3A) by ONp hydrolysis.

Physicochemical Characterization of Experimental Polymer Conjugates

UV–vis was used to measure the incorporation of MMC (365 nm) in the drug-containing precursor and FITC (495 nm) in the fluorescently labeled precursor using calibration curves for MMC and FITC, respectively. The MA-GG-ONp content of all precursors was assessed by absorbance measurements (400 nm) of hydrolytically released ONp. Following conjugation to the available ONp, absorbance measurements of polymer-incorporated RF (455 nm) and FA (365 nm) were determined using standard curves of the amine-functionalized ligands. The average molecular weight (M_w) and molecular weight distribution [polydispersity (n), calculated as average molecular weight (M_w)/number average molecular weight (M_n)] were estimated by size exclusion chromatography (SEC) on a Superose 12 column (10 mm × 30 cm) (Amersham Biosciences, Piscataway, NJ) using a fast protein liquid chromatography (FPLC) system (Amersham Biosciences) which was calibrated for poly (HPMA) fractions of known molecular weights.

Cell Culture

MCF-7 and SKBR-3 cells were obtained from American Type Culture Collection (Manasas, VA), and maintained at 37°C, under 5% CO_2 in DMEM and McCoy's 5a medium, respectively, (Invitrogen Life Technologies, Carlsbad, CA) supplemented with 10% fetal bovine serum, 1% nonessential amino acids, 100 U/ml penicillin, and 100 μg/ml streptomycin.

HPMA-FITC Copolymer-Ligand Internalization

MCF-7 and SKBR-3 cells were seeded at 5×10^5 cells/ml in 96-well plates and cultured until confluence prior to experimentation. Cells were washed twice with 200 μl pre-warmed HBSS, then incubated with 0–2,000 μg/ml weight eqv of nontargeted (P1) and RF- (P1-RF) or FA-

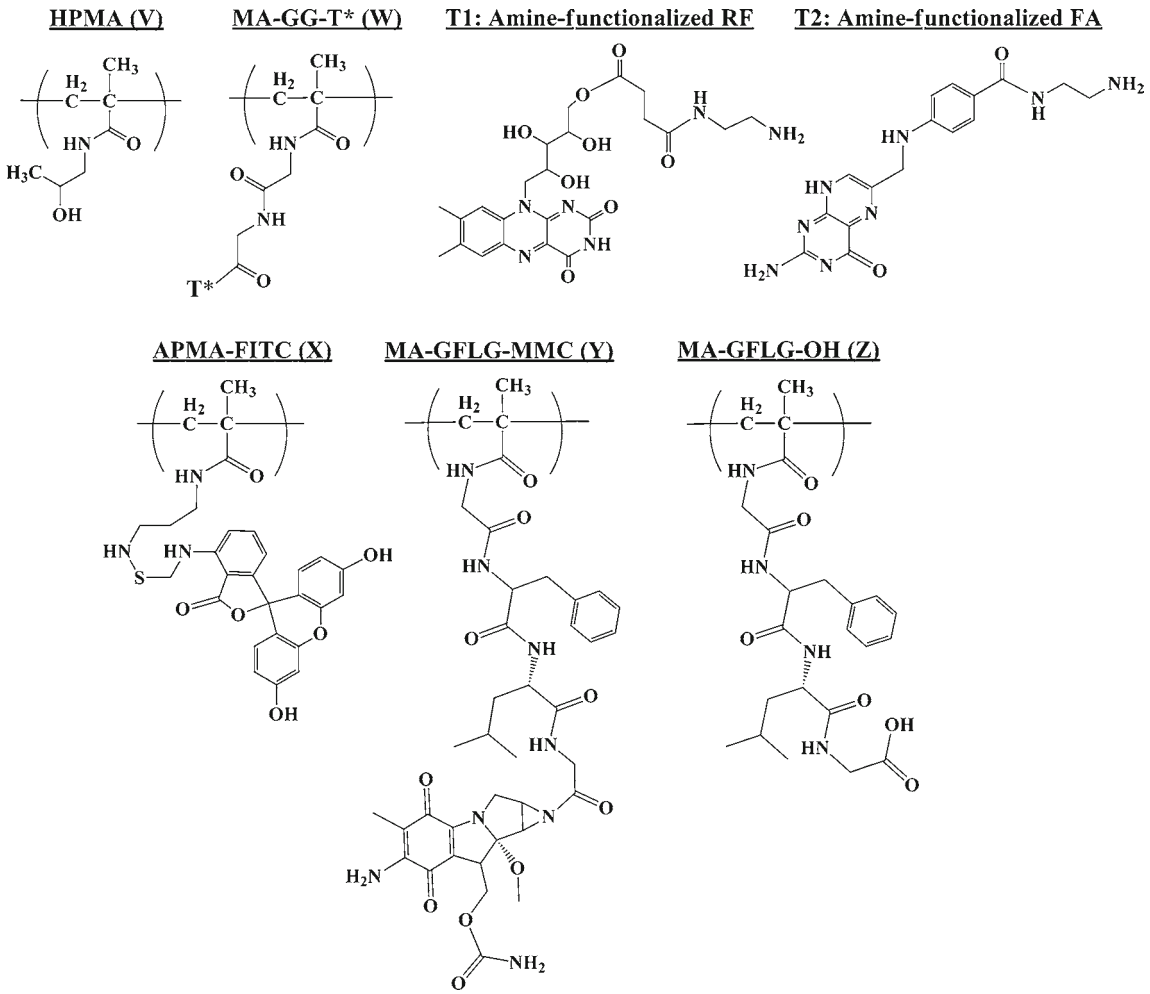

Fig. 1 Synthesis of HPMA polymer constructs. HPMA copolymer (*V*) and dipeptide-containing monomer (*W*) functionalized with T1 or T2 were copolymerized with FITC-conjugated monomer (*X*) or tetrapeptide-MMC monomer (*Y*) to produce the fluorescently-labeled and drug-containing polymer conjugates, respectively. Neutral control polymers were produced to yield nontargeted (GG-OH) and drug-lacking (GFLG-OH, *Z*) test conjugates.

(P1-FA) targeted FITC-labeled conjugates at 37°C for 1 h. Following incubations, cells were washed three times with pre-chilled DPBS pH 7.4 to remove uninternalized polymers, followed by a 5 min wash with pre-chilled DPBS pH 3 to remove all membrane-associated fractions which associate with membrane receptors at neutral pH. Cells were then lysed for 2 h in 1 N NaOH. The intrinsic FITC fluorescence (495/521 nm) within the conjugates was used to determine the amount of cell-associated FITC from a standard curve and results were standardized to total protein content. Intracellular FITC concentrations were then converted to the amount of internalized conjugate using the experimentally determined FITC content of the conjugate precursors. The affinity (k_m) and capacity (J_{max}) of RF- and FA-specific uptake was calculated using Michaelis-Menten kinetics following correction for nonspecific uptake of the nontargeted conjugate. Results were expressed as mean ± standard deviation (SD).

Competitive Uptake Studies

Studies were conducted in Costar® 24-well plates (Fisher Scientific, Pittsburg, PA) where MCF-7 cells were seeded at a density of 5×10^4 cells/cm^2 and used 3 days after seeding. Competitive uptake studies were conducted to determine the extent of RF-mediated uptake for targeted and nontargeted conjugates. Cells were incubated for 30 min with media solutions containing 10 nM [^{3}H]-RF (Moravek Biochemicals, Brea, CA) and 0–5,000 ng/ml wt eqv of RF-targeted (P2B, P2C) or nontargeted (P2A) conjugates. Cells were then washed three times with HBSS pH 7.4 and once with acidic HBSS pH 3 for 10 min to remove all nonspecific and membrane bound fractions. Following a 2 h cell lysis with 1 N NaOH, cell-associated radioactivity was measured with scintillation counting, and results were standardized to total protein content. Statistical analysis was conducted using a one-way analysis of variance (ANOVA) followed

by Newman-Keuls multiple comparison test. Results were expressed as mean ± SD.

Internalization of Free and Conjugated MMC

Non-radioactive uptake studies were conducted in a similar manner as explained above, in order to measure the cellular accumulation of MMC following passive and active internalization. MCF-7 cells were treated for 60 min with a 10 μg/mL MMC eqv of free and RF-targeted (P3B, P3C) or nontargeted (P3A) conjugates and then washed to remove un-internalized and membrane-associated MMC. In order to determine the effect of compartmental neutralization on the internalization of free and conjugated MMC, cells were pretreated for 30 min with 25 μM monensin or 300 μM primaquine (LKT Laboratories, St. Paul, MN) prior to MMC uptake studies. Cells not treated with monensin or primaquine were used as a control. Cell lysates were analyzed with UV spectroscopy to measure the absorbance of intracellular MMC (365 nm) which resulted for each treatment. The concentration of internalized MMC was extrapolated from a standard curve produced for this drug, and the results are presented as a percentage of the MMC internalization in the cells treated with the lysomotropic agents *versus* the untreated control. Statistical analysis was determined by ANOVA followed by Newman-Keuls multiple comparison test. Results were expressed as mean ± SD.

Immunofluorescence and Confocal Microscopy

MCF-7 cells were seeded 3 days prior to use at 5×10^3 cells/cm^2 in collagen-coated culture slides (BD Biosciences, Bedford, MA). Cells were treated with 20 μg/mL MMC eqv of free MMC and RF-targeted (P3B) or nontargeted (P3A) MMC-conjugates at 37°C for 10 min, 30 min, and 6 h. In order to prevent potential receptor saturation and modification to RF intracellular kinetics, RF-targeted trafficking was monitored with P3B conjugates which contain targeting ligand. Cells were then fixed, permeabilized, and blocked prior to immunolabeling for 2 h at RT with early endocytic (Rab5 GTPase) or lysosomal (LAMP-1) protein markers. Cells were then washed thoroughly and probed with AlexaFluor546-labeled sheep anti-mouse IgG (Molecular Probes, Eugene, OR) for 1 h. Nuclear labeling was conducted for 1 h using propidium iodide. Fluorescent samples were preserved using GelMount (Biomeda Corp., Foster City, CA) and visualized on a Nikon Eclipse TE2000 E inverted confocal laser scanning microscope equipped with two fixed lasers, 405 and 543 nm. The 3D images were acquired on Nikon EZ-C1 software (Gold v. 2.3, Image Systems Inc., Columbia, MD) using a 60× oil objective for parameters: 0.25 μm *z*-step, 6 μs scan dwell time, and the average of two scans per channel. Each image was iteratively deconvolved for both channels and analyzed for 3D colocalized regions using Volocity (v. 3.6, Improvision, Waltham, MA). The extent of colocalization between MMC (405 nm), following its free and RF-targeted or nontargeted conjugate administration, and protein markers (543 nm) was determined by calculating the percent of total overlapping volume between the two channels compared to the total drug volume. The data represents the average of three regions for each treatment, and statistical significance was determined using Pearson's correlation (PC).

In-Vitro Stability of HPMA Copolymer-RF-MMC Conjugates

RF-containing HPMA copolymer-MMC conjugate (P3B) was incubated in buffers designed to mimic the physiological and lysosomal environments in order to study the hydrolytic and enzymatic stability of spacers linking RF and MMC to the copolymers (Table IV). To investigate hydrolytic stability, 1 mg/ml of conjugate was dissolved in phosphate buffers of pH7.4 and 5.5, at 37°C. Enzymatic stability was determined in phosphate buffer pH5.5 containing 2 mM EDTA, 10 mM reduced glutathione, and 100 μg/ml human cathepsin B (EMD Biosciences, La Jolla, CA). At regular time intervals samples were taken and immediately stored at −80°C until analysis. Prior to analysis, all samples were eluted on desalting spin columns of 7 kD molecular weight cut off (Pierce Biotechnology, Rockford, IL) to obtain the polymer fraction. After elution, polymer and control samples were analyzed for RF (445 nm) and MMC (365 nm) content using UV–vis. The percent of bound RF and MMC remaining was determined from the total content in the original copolymers. Time-dependent release profiles were produced by nonlinear regression to calculate the half-lives associated with RF and MMC release in all incubation conditions.

Cytotoxicity Studies

The cytotoxicity of free and conjugated MMC was determined using the fluorescent (3-(4,5-Dimethylthiazol-2-yl)-2,5-diphenyltetrazolium bromide (MTT) assay, which is a standard colorimetric method for measuring the enzymatic activity of live cells. MCF-7 cells were seeded at 5×10^4 cells/mL in 96 well plates (USA Scientific, Ocala, FL) 1 day prior to experimentation. Cells were treated in culture medium for 72 h with 1–1,000 ng/mL MMC eqv of free and RF-targeted (P3B, P3C) and nontargeted (P3A) conjugates of MMC, RF eqv for targeted conjugates without MMC (P2B, P2C), or weight eqv for nontargeted conjugates without MMC (P and P2A). Following treatment, 5 mg/mL MTT was added to each well and incubated for 4 h. This solution was removed from each well prior to resuspension in DMSO for 1 h. Treatment solutions were analyzed for

absorbance of a reduced purple formazan MTT product (560 nm), which correlates to cell viability, and compared with that of positive (untreated) and negative (100% MeOH pretreated) controls. Dose–response curves were generated using a sigmoidal dose–response nonlinear curve fitting function (GraphPad Prism 5) to determine the concentration necessary to inhibit cell viability by 50% relative to nontreated control cells (IC_{50} dose).

RESULTS

Characterization of Polymeric Conjugates

Novel copolymer conjugates containing RF and MMC were synthesized to evaluate the targeting potential of RF for macromolecular chemotherapeutics. UV spectroscopy was used to analyze the FITC, MMC, and (GG)ONp content in each polymerized conjugate, as well as to determine RFl and FAl incorporation following conjugation to the derivatized targeting conjugates. Polymer content of each compound is listed in Table I.

An SEC/FPLC system was utilized for the separation and UV quantification of the weight average molecular weight (Mw) and polydispersity (n) of all final copolymer conjugates. Fluorescently-labeled conjugates (P1, P1-RF, P1-FA) showed similar molecular weight averages of 13–14 kD. Experimental conjugates without (P2A, P2B, P2C) and with (P3A, P3B, P3C) MMC displayed molecular weight averages between 19–33 kD, with the exception of HPMA homopolymer control (45 kD). The incremental increases in RF content for both the drug-containing (P3B, P3C) and control (P2B, P2C) conjugates exhibited an RF-dependent increase in molecular weight, which can likely be explained by differences in the hydrodynamic volumes of the conjugates containing the water-soluble vitamin. The polydispersity of all copolymer conjugates remained relatively consistent ($n = 1.26–1.54$).

Breast Cancer Cell Selectivity for Polymeric Conjugates

The extent of RF-specific conjugate internalization was measured in the human breast cancer cell lines MCF-7 and SKBR-3 and compared with that of FA-assisted conjugate uptake. The nonspecific endocytosis of nontargeted FITC-labeled conjugates (P1) was subtracted from the amount of RF- (P1-RF) and FA- (P1-FA) targeted FITC-conjugates in order to determine the extent of RF- and FA-specific internalization. RF-targeted conjugates showed appreciable accumulation within MCF-7 (50.86 ± 2.69 ng/mg protein/60 min) and SKBR-3 (83.29 ± 4.65) cells. FA-targeting enabled a similar amount of conjugate incorporation into SKBR-3 cells (58.70 ± 3.98) yet only half that in MCF-7 cells (27.62 ± 3.42). Conjugate internalization occurred with high affinity for RF-specific uptake in both MCF-7 (198.8 ± 36.85 μg/ml) and SKBR-3 (306.1 ± 30.03) cells, unlike that of the FA-targeted conjugates which showed similar affinity for internalization within SKBR-3 (150.4 ± 19.28) but not MCF-7 (903.7 ± 185.2) cells (Table II). MCF-7 cells were chosen for subsequent experiments due to the higher affinity for RF-targeted conjugate internalization and the lack of affinity for FA-targeted conjugates.

Table I Physicochemical Characterization of HPMA Copolymer Conjugates

	Feed Comonomer Content					Polymer Characteristics					
Sample[a]	HPMA	GG-ONp	GFLG-OH	GFLG-MMC	APMA-FITC	FITC (mmol/g polymer)	RF (mmol/g polymer)	FA (mmol/g polymer)	MMC (mmol/g polymer)	Estimated Mw (kD)	Mw/Mn (n)
P1	88	10	0	0	2	0.12	0	0	0	13.0	1.42
P1-RF	88	10	0	0	2	0.12	0.56	0	0	14.6	1.30
P1-FA	88	10	0	0	2	0.12	0	0.51	0	14.3	1.37
P	100	0	0	0	0	0	0	0	0	44.7	1.51
P2A	85	10	5	0	0	0	0	0	0	24.0	1.49
P2B	85	10	5	0	0	0	0.48	0	0	19.4	1.54
P2C	85	10	5	0	0	0	0.84	0	0	20.9	1.50
P3A	85	10	0	5	0	0	0	0	0.61	24.7	1.42
P3B	85	10	0	5	0	0	0.46	0	0.61	30.2	1.48
P3C	85	10	0	5	0	0	0.87	0	0.61	33.6	1.26

[a] The sample identification codes correspond to the following copolymer conjugates: P1 = HPMA-GGOH-APMAFITC; P1-RF = HPMA-GGRF-APMAFITC; P1-FA = HPMA-GGFA-APMAFITC; P = HPMA homopolymer; P2A = HPMA-GGOH-GFLGOH; P2B = HPMA-GGRF↓-GFLGOH; P2C = HPMA-GGRF↑-GFLGOH; P3A = HPMA-GGOH-GFLGMMC; P3B = HPMA-GGRF↓-GFLGMMC; P3C = HPMA-GGRF↑-GFLGMMC; RF↓ = low (0.4 mmol/g polymer) RF content; RF↑ = high (0.8 mmol/g polymer) RF content

Table II Internalization Kinetics of HPMA Copolymer-FITC-Ligand Conjugates in Human Breast Cancer Cells

Treatment	Internalization Kinetics	
	k_m (μg/ml)	J_{max} (ng/60 min)
MCF-7		
P1-RF	198.8 ± 36.85	50.86 ± 2.69
P1-FA	903.7 ± 185.2	27.62 ± 3.42
SKBR-3		
P1-RF	306.1 ± 30.03	83.29 ± 4.65
P1-FA	150.4 ± 19.28	58.70 ± 3.98

RF-Competed Conjugate Internalization

In order to demonstrate active receptor-mediated targeting of RF-containing conjugates, competitive internalization studies with radiolabeled RF were conducted. Table III depicts the IC_{50} values associated with RF-competed internalization of nontargeted (P2A) and RF-targeted (P2B, P2C) conjugates. Incubation with the nontargeted P2A copolymer exhibited negligible inhibition of radiolabeled RF uptake within the concentration range tested. RF-targeted polymers exhibited potent IC_{50} values, which were positively-associated with increasing RF content (P2B = 198.4, P2C = 127.2 ng/mL). Based on these data and earlier studies (32), we concluded that functionalizing RF *via* its ribityl side chain enabled the retention of RF binding affinity for its cell-surface machinery.

Cellular Accumulation of MMC

To determine the extent of RF-mediated MMC internalization, MCF-7 cells were incubated for 60 min with 10 μg/mL MMC eqv of free and RF-targeted (P3B, P3C) or nontargeted (P3A) conjugates to allow both passive and active internalization, respectively. Results revealed that MMC cytosolic accumulation was significantly higher following the active internalization of the nontargeted (P3A: 2.31 ng/mg protein) and RF-targeted (P3B: 5.13 and P3C: 7.65 ng/mg protein) conjugates, as compared to that following the passive diffusion of free MMC (1.32 ng/mg protein) (Fig. 2). The difference between RF-targeted (specific + nonspecific) and nontargeted (nonspecific) MMC internalization reflects the amount of MMC internalized specifically by RF-mediated endocytosis. The resulting differences (2.82 and 5.34 ng/mg protein) indicate that RF-mediated conjugate internalization is an efficient and selective method of drug entry into breast cancer cells.

Following endocytosis, internalized material is contained in membrane-bound vesicles which shuttle through an endolysosomal pathway, characterized by increasing compartmental acidification. This cellular processing pathway results in the dissociation of receptor-ligand complexes and subsequent receptor membrane recycling for continuous ligand internalization (33). Biochemical modification of vesicular pH was induced to determine the role of compartmental acidification in the internalization of free and conjugated MMC. The lysosomotropic agents monensin and primaquine work through different mechanisms to neutralize the normally acidic (pH5–6) subcellular compartments which govern the intracellular trafficking of endocytosed material, namely the endosomes, lysosomes, and golgi. The intracellular accumulation of conjugated MMC, both RF-targeted and nontargeted, was significantly decreased upon vesicular neutralization (Fig. 3). The RF-mediated internalization of MMC, for both RF-containing conjugates (P3B and P3C), was abolished with monensin (1.98 and 1.60% untreated control) and primaquine (1.18 and 1.14%) treatment, which was similar for that of the nontargeted conjugate (P3A) (7.76 and 6.11%). The uptake of free MMC was

Table III Competitive Internalization of RF against Free RF and RF-targeted or Nontargeted Polymer Conjugates in MCF-7 Cells

Sample	Content	IC_{50} (ng/mL)
P2A	HPMA-GGOH-GFLGOH	NA[a]
P2B	HPMA-GGRF(0.48)-GFLGOH	198.4 ± 15.5
P2C	HPMA-GGRF(0.84)-GFLGOH	127.2 ± 10.3
RF	free RF	46.9 ± 5.3

[a] Competitive uptake against RF was negligible within the concentration range tested

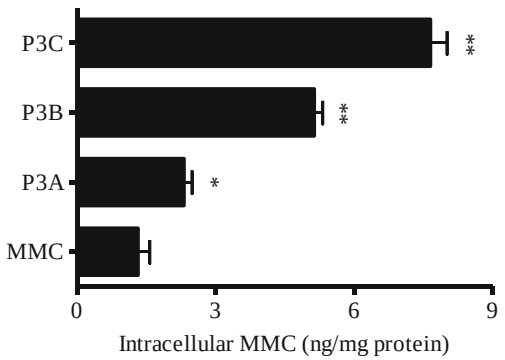

Fig. 2 Cellular accumulation of MMC following free and RF-targeted or nontargeted conjugate administration. MCF-7 cells were incubated with 10 μg/mL MMC eqv of free MMC, nontargeted MMC conjugate (P3A), or RF-targeted conjugates (P3B and P3C). The intracellular MMC concentration for each treatment was determined by UV analysis, calibrated to MMC standards, and standardized to total protein content. * $p < 0.05$, ** $p < 0.001$.

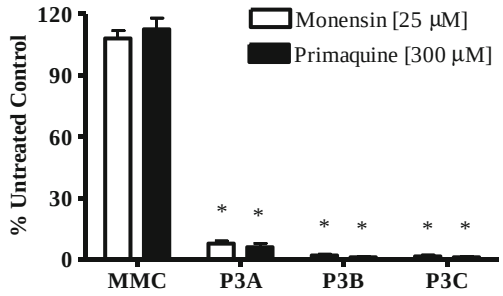

Fig. 3 Effect of endosomal neutralization on the internalization of free or polymer-bound MMC. MCF-7 cells were treated with 25 μM monensin (*open bar*) or 300 μM primaquine (*solid bar*) with 10 μg/mL MMC eqv of free MMC, nontargeted MMC conjugate (P3A), and RF-targeted conjugates (P3B and P3C). Cell lysates were analyzed for intracellular MMC content with UV spectroscopy. Results are presented as the percentage of the untreated (monensin and primaquine-free) control. * $p < 0.001$.

not significantly affected by either treatment. Results confirm that the cellular uptake of polymer-conjugated MMC is confined to endocytic processes.

Conjugate Trafficking Along the Endolysosomal System

In order to illustrate the spatial and temporal trafficking of free and polymer-conjugated MMC along vesicular and nuclear compartments, the inherent fluorescence of MMC was monitored for its 3D colocalization with fluorescently labeled early endosome (Rab5), lysosome (LAMP-1), and nuclear (propidium iodide) fluorescent markers (Fig. 4), over a 6 h period. The extent of colocalization was quantified at each time point using a minimum of three regions using Pearson's correlation (PC) to calculate the percent of early endosome, lysosome, and nuclear fluorescent volumes which overlapped with the total MMC fluorescent volume (Fig. 5). For each marker, the percent overlap of nontargeted (P3A) and RF-targeted (P3B) MMC-conjugate was compared to that of free MMC, and significant differences were expressed at each time point.

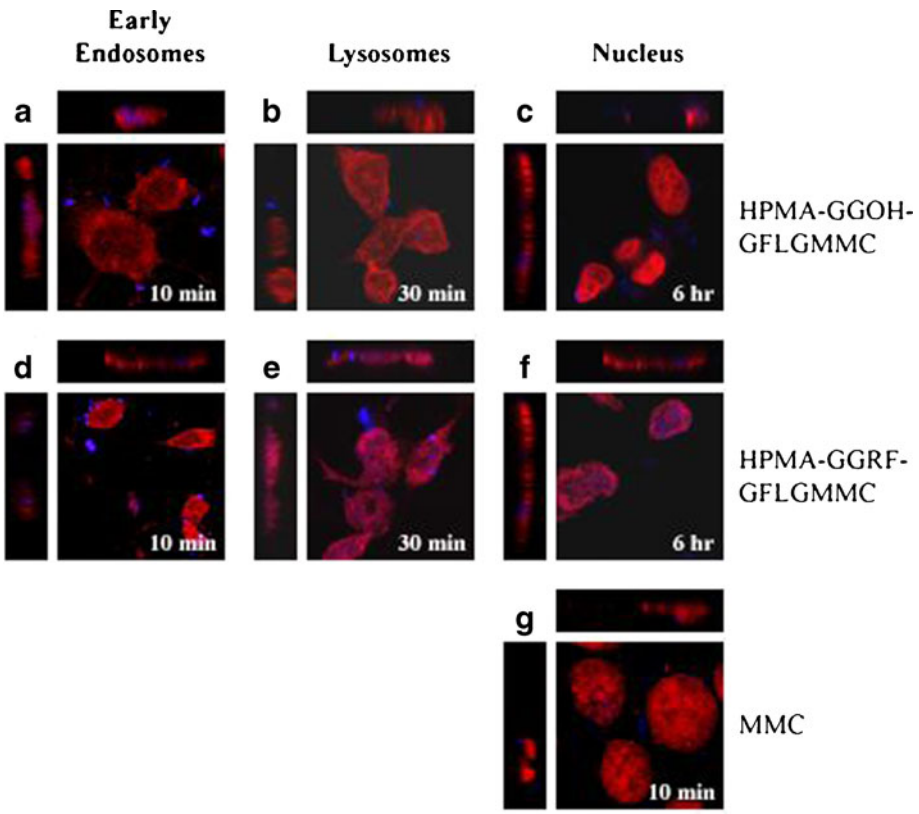

Fig. 4 Subcellular co-localization of free and nontargeted- (P3A) or RF-targeted- (P3B) conjugate (*blue*) with early endocytic (Rab5 GTPase), lysosomal (LAMP-1), and nuclear (propidium iodide) protein markers (*red*) in MCF-7 cells. The inset view defines the XY plane, the left panels represent the YZ, and the top panels represent the XZ planes. The nontargeted MMC-conjugate (P3A) associated with an early endosomal compartment within 10 min (**a**), followed by movement to lysosomal (**b**) and nuclear (**c**) compartments at 30 min and 6 h, respectively. The RF-targeted MMC-conjugate (P3B) was rapidly endocytosed to allow for localization to early endosomes within 10 min (**d**) and lysosomes (**e**) within 30 min. Maximum MMC-nuclear overlap resulted from longer incubation, up to 6 h, with RF-targeted MMC-conjugate (P3B) (**f**). Unconjugated MMC rapidly diffused, within 10 min, into cell nuclei (**g**) and exhibited minimal fluorescent colocalization with endocytic markers (not shown).

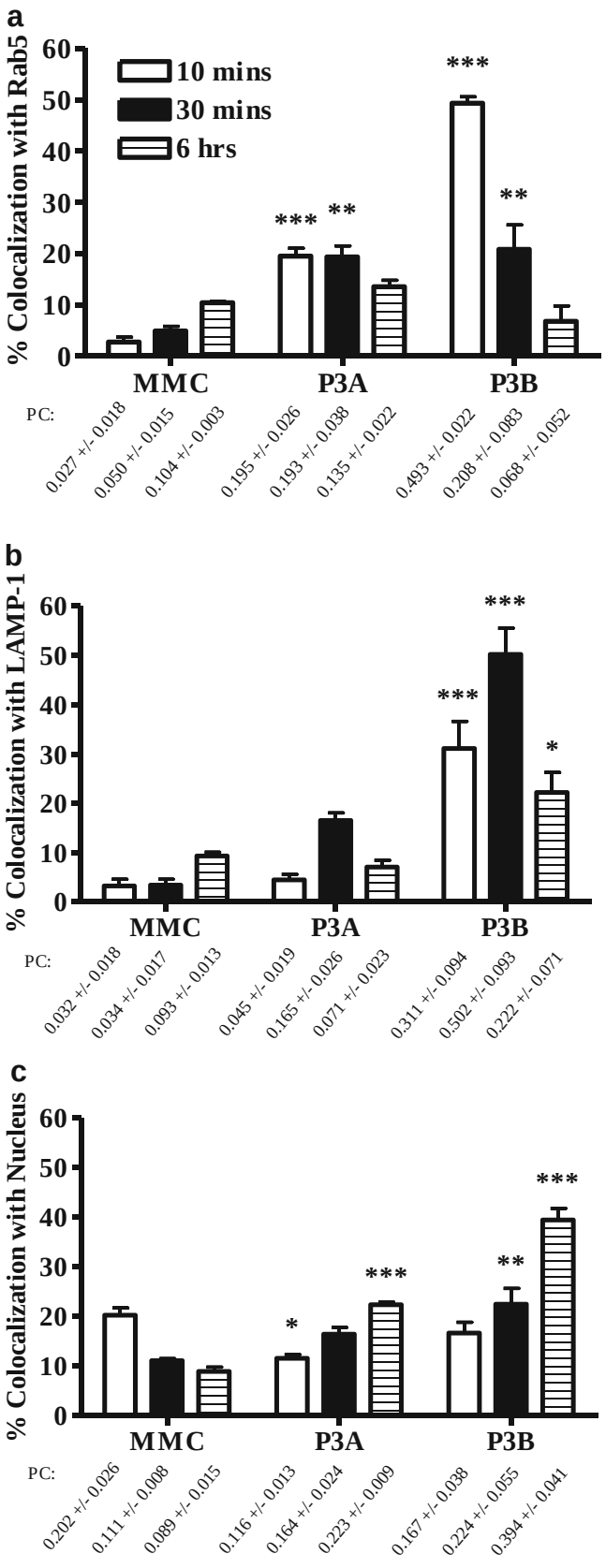

Fig. 5 Quantification of the colocalization of free MMC and RF-targeted (P3B) or nontargeted (P3A) MMC-conjugates with early endosomal (**a**), lysosomal (**b**), and nuclear (**c**) compartments in MCF-7 cells after 10 min (open bar), 30 min (solid bar), or 6 h (striped bar). The extent of MMC colocalization with each marker was determined using Pearson's correlation. Results are the mean ± SD (n = 3). Nontargeted (P3A) and RF-targeted (P3B) MMC-conjugate colocalization with each marker was compared to that of free MMC at each time point. * $p < 0.01$, ** $p < 0.005$, *** $p < 0.001$.

Following endocytic internalization, vesicles containing MMC-conjugates displayed a time-dependent movement along the endolysosomal system. Nontargeted MMC-polymers rapidly associated with early endosomes within 10 min (Fig. 4a) where they remained consistently localized (13.5 to 19.5%) over a 6 h period (Fig. 5a). Similarly, RF-targeted drug conjugates immediately assembled in apical endosomal compartments (Fig. 4d) but to a significantly greater extent (~ 4-fold) than the nontargeted complexes. Free MMC showed minimal retention within early endosomes; however, results display an increasing trend with longer exposure (Fig. 5a). Both nontargeted and RF-targeted drug conjugates followed similar intracellular sorting pathways ultimately leading to lysosomal compartments where the highest extent of colocalization occurred following 30 min (16.5 and 50.2%) of vesicular trafficking. Free MMC displayed negligible accumulation (~ 3%) within lysosomes during brief incubations, although longer exposure promoted the pH-dependent ion-trapping (~ 10%) inside the acidic organelles (Fig. 5b).

The prolonged retention of MMC-containing polymers within digestive lysosomal compartments permitted the enzymatic recognition of polymer-associated GFLG substrates by cathepsin B and subsequent release of intact MMC from these polymer-peptide linkers (34). Immediately following release, MMC is directed along a concentration gradient for diffusion into the cytosol from which nuclear trafficking will occur. Once in the nucleus, MMC is bioreductively activated to function as a potent DNA-alkylating agent leading to a high degree of DNA crosslinking and acute cytotoxic effects (35). A considerable amount of polymer-liberated MMC concentrated in nuclei within 30 min; however, 6 h treatments supported significantly higher nuclear accumulation of RF-targeted (39.4%) and nontargeted (22.3%) conjugate-administered MMC. Alternatively, incubation with free drug illustrated maximum MMC-nuclear overlap during only 10 min (20.2%) of passive drug diffusion at which time drug equilibration between the intra- and extra-nuclear environment suggestively prevented further nuclear localization of drug molecules (Fig. 5c).

Controlled Enzymatic Release of Intact MMC

The hydrolytic stability of RF-containing HPMA-MMC conjugate (P3B) was tested in conditions representative of extracellular, pH 7.4, and lysosomal, pH 5.5, environments. The results demonstrate the hydrolytic resistance of both Gly-Gly and Gly-Phe-Leu-Gly linkages for RF and MMC, respectively, at neutral pH. Upon incubation in acidic buffer, RF ($t_{1/2}$ = 59.22 ± 6.74 h) and MMC ($t_{1/2}$ = 45.61 ± 9.31 h) were slowly released from their peptidyl spacers at a rate that correlated with increasing peptide length. The enzymatic stability of P3B conjugates were investigated in buffer of pH 5.5 containing cathepsin B in order to measure the efficiency of drug release from the polymer-peptide enzyme substrate. Data revealed the rapid release of MMC ($t_{1/2}$ = 3.99 ± 1.97 h) from polymer-contained GFLG spacers, whereas RF ($t_{1/2}$ = 65.49 ± 7.88 h) release occurred at a rate similar to that in acidic medium. Results are reported in Table IV.

MMC-Induced Cytotoxicity

Cytotoxicity of experimental and control polymers was determined using the MTT assay, where fluorescence detection of a reduced formazan product is used to measure the enzymatic activity in viable cells. In order to demonstrate that the cytotoxic effect of the MMC conjugates was not influenced by the drug delivery vehicle, control polymers of HPMA (P) and RF-targeted (P2B and P2C) or nontargeted (P2A) HPMA systems without drug were included. All control polymers exhibited negligible cytotoxicity within the concentration range tested, suggesting the biocompatible nature of HPMA, RF, and peptide linkers, in MCF-7 cells. MMC-induced cytotoxicity was measured for free and RF-targeted (P3B and P3C) and nontargeted MMC conjugates (P3A). High cytotoxic potencies were exhibited by all MMC treatment groups (Fig. 6); however, free MMC elicited the lowest effective dose (IC_{50} = 0.05 μg/mL). This may be the result of the additional time required for conjugate internalization, lysosomal drug release, and nuclear drug localization. Increasing the RF content in targeted polymers resulted in an RF-dependent decrease in the IC_{50} dose (0.21–0.10 μg/mL). P3A did exhibit appreciable MMC-induced cytotoxic effect (IC_{50} = 0.61 μg/mL), but to a lesser extent than free and RF-targeted MMC. Although the cytotoxic potency of RF-targeted MMC conjugates was less than that of free MMC, apoptotic analysis following 72 h treatments displayed equivalent cell death (> 95%).

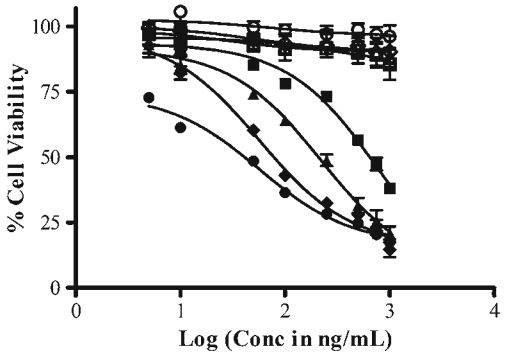

Fig. 6 Cytotoxicity of free MMC and polymer conjugates after treatment with free MMC (*closed circle*), nontargeted (P3A, *closed square*), or RF-targeted (P3B and P3C, *closed triangle and diamond*) conjugates in MCF-7 cells. MMC-free conjugates' (P1, *open circle*; P2A *open square*; P2B, *open triangle*; P2C, *open diamond*) cytotoxicity were negligible in the concentration range tested. Using nonlinear sigmoidal dose response curve fitting (GraphPad Prism 5), the mean ± SD IC_{50} values obtained were 0.05 ± 0.02, 0.61 ± 0.03, 0.21 ± 0.02, and 0.10 ± 0.02 μg/mL for MMC, P3A, P3B, and P3C, respectively.

Table IV Hydrolytic and Enzymatic Release Rates of RF and MMC from Polymer Peptide Linkages

Treatment Conditions	Release Half-life ($t_{1/2}$, hr)	
	RF	MMC
pH 7.4	NA[a]	NA[a]
pH 5.5	59.22 ± 6.74	45.61 ± 9.31
pH 5.5 + Cathepsin B	65.49 ± 7.88	3.99 ± 1.97

[a] Compound release was negligible (< 5%) during 72 h incubation

DISCUSSION

Pharmaceutical nanocarriers have been successfully employed to enhance the locoregional delivery of conventional anticancer agents. Carrier conjugation prevents the promiscuous diffusion of cytotoxic compounds into healthy and cancerous tissues consequently prolonging the drugs' residence time in blood circulation and exposure to the EPR effect characteristic of the neovasculature supporting solid tumors. Targeting the macromolecular conjugates with the aid of ligands specific to cell-surface receptor proteins allows for the highly-selective delivery of therapeutics to target cancer cells. Unlike normal tissues, the majority of tumor types overexpress certain vitamin membrane receptors although the degree of overexpression varies not only between each cancer form but also among the various stages of tumor progression (7). Research into vitamin-targeted chemotherapy has advocated its promising clinical utility; however, the differential regulation of vitamin receptors mandates further investigations to determine the most efficacious targeting approach for each type of cancer tissue. The present study was initiated to investigate a novel targeting strategy using RF for chemotherapeutic delivery to breast cancer tissue, where RF has been recognized as an important regulatory factor. Recent analyses determined that the high-affinity receptor-assisted

internalization of RF (17,19,36,37) is significantly upregulated in breast cancer tissue (20), possibly explaining the dramatic decrease in RF serum levels of breast cancer patients (16).

Preliminary studies were conducted to measure the ligand-selectivity of RF-targeted polymers in an estrogen-dependent (MCF-7) and independent (SKBR-3) breast cancer cell model and compared with that of the well characterized targeting vitamin folic acid (5,38). Findings illustrate the high-affinity internalization of RF-conjugates in both MCF-7 and SKBR-3 cells, whereas FA-selectivity was maintained only by SKBR-3 cells. The extent of polymer internalization was comparable for the high-affinity endocytic processes mediated by RF and FA; however, the low-affinity incorporation of FA-polymers was considerably less in MCF-7 cells (Table II). Similar variability in ligand-specificity of breast cancer cells was previously demonstrated for FA (9), cobalamin (39), and hyaluronan (40). Although further investigations are necessary to be conclusive, results from this comparative analysis suggest a highly reliable and efficacious targeting role for RF in breast cancer-directed drug delivery.

In order to measure the extent of RF-specific internalization, P2 polymers were prepared for analysis in competitive uptake studies with tritiated RF. RF-targeted polymers potently inhibited radiolabeled-RF uptake in a manner positively associated with polymer RF content (Table III). These results ensured that RF retained high affinity for RF cell surface machinery following polymer-peptide conjugation facilitating the receptor-specific internalization of targeted conjugates. Nontargeted conjugates showed negligible competition for RF-specific internalization within the physiological RF concentration range suggesting internalization occurred predominantly *via* a nonspecific or passive endocytic mechanism.

The biocompatible copolymer HPMA was employed as a multifunctional vehicle which offers facile tailoring to suit specific drug targeting needs (22). Clinically, it is important that a macromolecular prodrug remain stable during blood circulation, but the cytotoxic drug will need to be released from carrier complexes following endocytic internalization. Shuttling along cytoskeletal networks, vesicular cargo trafficks to endolysosomal compartments where the large complexes will be metabolized. An array of oligopeptides have been designed for proteolytic degradation by lysosomal proteases, particularly the tetrapeptide Gly-Phe-Leu-Gly (GFLG) which serves as a substrate for cathepsin B, an enzymatic protein located in the lysosome (41). In the present study RF and MMC were stably attached to the dipeptide Gly-Gly and tetrapeptide GFLG, respectively, at neutral pH. Although both RF and MMC were slowly freed from their peptidyl spacers in acidic conditions, MMC release occurred slightly faster indicating the increased accessibility of the longer tetrapeptide for hydrolysis. Previous studies have indicated that a peptide spacer with a terminal hydrophobic amino acid may enhance the hydrolytic stability of the MMC linkage (34); therefore, additional studies are necessary to select the peptidyl spacer which would promote optimal resistance to extracellular hydrolysis yet enable maximum lysosomal cleavage. The secondary amide conjugation of MMC to the terminal glycine of polymer-GFLG side chains permitted its efficient recognition and rapid cleavage by the lysosomal enzyme cathepsin B (Table IV) at a rate similar to that seen for previously investigated poly-N-(2-hydroxyethyl)-l-glutamine (PHEG)-polypeptide-MMC conjugates (42). Combined, data from the *in-vitro* stability and fluorescent colocalization studies suggest that the intracellular trafficking of RF-targeted HPMA-MMC conjugates promotes the highly controlled release of intact MMC and subsequent diffusion into nuclei where it will exert its anticancer effect.

The *in-vitro* efficacy of RF-targeted MMC-conjugates (P3 polymers) was analyzed in MCF-7 cells, where RF-targeting appears to be more sensitive. The anticancer agent MMC was chosen as the proof-of-principle drug because it is an extremely potent cytotoxin in breast cancer tissue (43) but is rarely administered as a monotherapy due to the delayed cumulative myelosuppression resulting from its unavoidable accumulation in bone marrow (25). Low molecular weight chemotherapeutics rapidly diffuse across cell membranes, with the assistance of an intracellular concentration gradient, until equilibration between the extra- and intracellular compartments at which point drug influx ceases. Macromolecular delivery limits drug internalization to active endocytic processes, which occur in a concentration-independent manner afforded by cellular energy supplies. Unlike the nonspecific pinocytic capture of nontargeted complexes, ligand-targeted conjugates serve as high-affinity substrates for specific membrane proteins which assist in their preferential receptor-mediated endocytic entry. Cellular uptake studies were conducted to measure the cellular accumulation of MMC following 60 min treatments with free and RF-targeted or nontargeted conjugates. The active internalization of polymeric-MMC resulted in significantly higher intracellular MMC concentrations, most notably for RF-targeted conjugates, compared to the passive diffusion of free MMC (Fig. 2). Although endocytosis occurs much slower than simple diffusion, the direct binding and signaling events associated with receptor-mediated entry promote the immediate internalization of ligand-targeted drug conjugates. Similar results were previously shown for macromolecular-MMC conjugates in a variety of cancer cell lines (34,44).

Several polymer-based delivery vehicles have been found to disrupt the membrane integrity of epithelial cells (45). In order to ensure the increase in cell-associated MMC resulted from the active internalization of polymeric-MMC, cellular uptake studies were also conducted in the presence of

lysosomotropic agents which are known to significantly hamper the endocytic internalization and intracellular sorting of receptor-bound ligands. Following internalization, vesicular cargo is guided through an endosomal maturation process, characterized by increasing intravesicular acidity (pH 7–5) (8). Endosomal acidification promotes the dissociation of ligand-receptor complexes to allow for the tightly-regulated intracellular processing of individual ligands and the efficient receptor recycling to apical membranes (20). Modification to this intracellular event results in the cytosolic build-up of endocytosed complexes which limits membrane-receptor availability and prevents further ligand internalization (46–48). Biochemical modification with both monensin and primaquine completely abolished (> 95%) the cellular accumulation of polymeric-MMC while the passive uptake of free MMC remained unaffected (Fig. 3), ruling out the possibility of intracellular conjugate leaking.

The intracellular trafficking of the HPMA-MMC conjugates was monitored using confocal microscopy (Fig. 4) and quantified for the extent of fluorescent 3D colocalization of drug with endocytic and nuclear compartments (Fig. 5). RF-targeted and nontargeted MMC-conjugates displayed similar trafficking profiles along endolysosomal machinery; however, the extent of MMC colocalization with all compartments was significantly greater for RF-directed polymers. Following vesicular internalization, MMC-conjugates quickly shuttled through early endosomal compartments prior to their localization in lysosomal compartments within 30 min. The diffusion of free MMC resulted in its rapid nuclear localization within 10 min, during which its association with early endosomes and lysosomes was negligible. Interestingly, the nuclear accumulation of free MMC decreased during longer incubations and displayed an increasing trend in endosome and lysosome localization. MMC diffusion into acidic organelles may have resulted from its prolonged cystolic residence (49), where the ionization of weak bases, such as MMC, will be trapped (50). Although conjugates required longer incubation, up to 6 h, for the lysosomal cleavage of MMC from the polymer-peptide backbone, the diffusion of polymer-released MMC led to a significantly higher extent of nuclear localization.

Cytotoxic analysis of all control polymers ensured the biocompatibility of our RF-containing HPMA-peptide delivery system. Upon comparison with previously investigated MMC-conjugates (44,51), nontargeted HPMA copolymer-MMC conjugates exhibited equivalent cytotoxic potency (IC_{50} ~ 0.6 μg/mL) in breast cancer cells. The RF-assisted internalization of MMC-conjugates significantly enhanced MMC sensitivity in MCF-7 cells in a manner which was positively associated with increasing polymer-RF content (IC_{50} = 0.21–0.1 μg/mL). Although unconjugated MMC was the most potent cytotoxic treatment in these cells (Fig. 6), it is important to note that this effect would not be limited to breast cancer tissue in an *in-vivo* system, and the IC_{50} values of the conjugates are still within an acceptable range for therapy.

In summary, RF-targeted therapeutics show considerable potential for the treatment of breast cancer. RF-targeted macromolecules exhibited high affinity for the RF-specific cell-surface machinery in MCF-7 cells, enabling the enhanced internalization of MMC. RF-targeted conjugates shuttled MMC along the intracellular endolysosomal network for the bioresponsive release and nuclear trafficking of MMC. Although RF-mediated internalization occurs slower than the passive diffusion of free drug, this process is far more selective (52). Data from these studies advocates further *in-vitro* and *in-vivo* characterizations in order to optimize the targeting efficiency of the highly-selective breast cancer targeting moiety RF.

CONCLUSION

Ligand-targeted therapeutics offer promising potential in the future of chemotherapy, as indicated by the increasing amount of these systems in Phase 2 and 3 clinical trials (2,22). Each system has been uniquely developed, *via* targeting ligand selection, for the highly selective delivery of anticancer agents to certain cancer types. The present study for the first time demonstrates the potential utility of RF as a targeting agent for breast cancer-directed therapeutics. Comparative analysis of the breast cancer cell selectivity for previously investigated targeting ligands indicates a more specific and effective targeting pathway for the RF system. Future investigations will aim to optimize the physicochemical parameters of RF-targeted systems, including drug and RF content. Furthermore, we would evaluate the RF-specific biorecognition and internalization of drug conjugates within other tissue systems, including the liver and small intestines, where RF cellular processing is also enhanced.

REFERENCES

1. Andersson L, Davies J, Duncan R, Ferruti P, Ford J, Kneller S, *et al.* Poly(ethylene glycol)-poly(ester-carbonate) block copolymers carrying PEG-peptidyl-doxorubicin pendant side chains: synthesis and evaluation as anticancer conjugates. Biomacromolecules. 2005;6:914–26.
2. Duncan R. The dawning era of polymer therapeutics. Nat Rev Drug Discov. 2003;2:347–60.
3. Tanaka T, Shiramoto S, Miyashita M, Fujishima Y, Kaneo Y. Tumor targeting based on the effect of enhanced permeability and retention (EPR) and the mechanism of receptor-mediated endocytosis (RME). Int J Pharm. 2004;277:39–61.
4. Mamot C, Drummond DC, Hong K, Kirpotin DB, Park JW. Liposome-based approaches to overcome anticancer drug resistance. Drug Resist Updat. 2003;6:271–9.

5. Reddy JA, Westrick E, Vlahov I, Howard SJ, Santhapuram HK, Leamon CP. Folate receptor specific anti-tumor activity of folate-mitomycin conjugates. Cancer Chemother Pharmacol. 2006;58:229–36.
6. Duncan R. Designing polymer conjugates as lysosomotropic nanomedicines. Biochem Soc Trans. 2007;35:56–60.
7. Russell-Jones G, McTavish K, McEwan J, Rice J, Nowotnik D. Vitamin-mediated targeting as a potential mechanism to increase drug uptake by tumours. J Inorg Biochem. 2004;98:1625–33.
8. Bareford LM, Swaan PW. Endocytic mechanisms for targeted drug delivery. Adv Drug Deliv Rev. 2007;59:748–58.
9. Parker N, Turk MJ, Westrick E, Lewis JD, Low PS, Leamon CP. Folate receptor expression in carcinomas and normal tissues determined by a quantitative radioligand binding assay. Anal Biochem. 2005;338:284–93.
10. Garnett MC. Targeted drug conjugates: principles and progress. Adv Drug Deliv Rev. 2001;53:171–216.
11. Qian ZM, Li H, Sun H, Ho K. Targeted drug delivery *via* the transferrin receptor-mediated endocytosis pathway. Pharmacol Rev. 2002;54:561–87.
12. Paulos CM, Reddy JA, Leamon CP, Turk MJ, Low PS. Ligand binding and kinetics of folate receptor recycling *in vivo*: impact on receptor-mediated drug delivery. Mol Pharmacol. 2004;66:1406–14.
13. Salazarand MD, Ratnam M. The folate receptor: what does it promise in tissue-targeted therapeutics? Cancer Metastasis Rev. 2007;26:141–52.
14. Castrellonand AB, Gluck S. Chemoprevention of breast cancer. Expert Rev Anticancer Ther. 2008;8:443–52.
15. Karande AA, Sridhar L, Gopinath KS, Adiga PR. Riboflavin carrier protein: a serum and tissue marker for breast carcinoma. Int J Cancer. 2001;95:277–81.
16. Vaidya SM, Kamlakar PL, Kamble SM. Molybdenum, xanthine oxidase and riboflavin levels in tamoxifen treated postmenopausal women with breast cancer. Indian J Med Sci. 1998;52:244–7.
17. Mason CW, D'Souza VM, Bareford LM, Phelps MA, Ray A, Swaan PW. Recognition, co-internalization, and recycling of an avian riboflavin carrier protein in human placental trophoblasts. J Pharmacol Exp Ther. 2006;317:465–72.
18. Yonezawa A, Masuda S, Katsura T, Inui KI. Identification and functional characterization of a novel human and rat riboflavin transporter, RFT1. Am J Physiol Cell Physiol. 2008;295:C632–41.
19. Huangand SN, Swaan PW. Involvement of a receptor-mediated component in cellular translocation of riboflavin. J Pharmacol Exp Ther. 2000;294:117–25.
20. Bareford LM, Phelps MA, Foraker AB, Swaan PW. Intracellular processing of riboflavin in human breast cancer cells. Mol Pharm. 2008;5:839–48.
21. D'Souza VM, Foraker AB, Free RB, Ray A, Shapiro PS, Swaan PW. cAMP-Coupled riboflavin trafficking in placental trophoblasts: a dynamic and ordered process. Biochemistry. 2006;45:6095–104.
22. Kopecek J, Kopeckova P, Minko T, Lu Z. HPMA copolymer-anticancer drug conjugates: design, activity, and mechanism of action. Eur J Pharm Biopharm. 2000;50:61–81.
23. Noriand A, Kopecek J. Intracellular targeting of polymer-bound drugs for cancer chemotherapy. Adv Drug Deliv Rev. 2005;57:609–36.
24. Rihovaand B, Kubackova K. Clinical implications of N-(2-hydroxypropyl)methacrylamide copolymers. Curr Pharm Biotechnol. 2003;4:311–22.
25. Bradner WT. Mitomycin C: a clinical update. Cancer Treat Rev. 2001;27:35–50.
26. Strohalmand J, Kopecek J. Poly N-(2-hydroxypropyl) methacrylamide. 4. Heterogeneous polymerization. Makromol Chem. 1978;70:109–18.
27. Kopeček J, Rejmanová P, Strohalm J, Ulbrich K, Říhová B, Chytrý V, Lloyd JB, Duncan R. Synthetic polymeric drugs. US Patent. 5, 037, 883. Aug 6, 1991. p. 883.
28. Rejmanova P, Labsky J, Kopecek J. Aminolyses of monomeric and polymeric p-nitrophenyl esters of methacryloylated amino acids. Makromol Chem. 1977;178:2159–68.
29. Omelyanenko V, Kopeckova P, Gentry C, Kopecek J. Targetable HPMA copolymer-adriamycin conjugates. Recognition, internalization, and subcellular fate. J Control Release. 1998;53:25–37.
30. Mitra A, Nan A, Ghandehari H, McNeill E, Mulholland J, Line BR. Technetium-99m-Labeled N-(2-hydroxypropyl) methacrylamide copolymers: synthesis, characterization, and *in vivo* biodistribution. Pharm Res. 2004;21:1153–9.
31. Luo J, Smith MD, Lantrip DA, Wang S, Fuchs PL. Efficient syntheses of pyrofolic acid and pteroyl azide, reagents for the production of carboxyl-differentiated derivatives of folic acid. J Am Chem Soc. 1997;119:10004–13.
32. Phelps MA, Foraker AB, Gao W, Dalton JT, Swaan PW. A novel rhodamine-riboflavin conjugate probe exhibits distinct fluorescence resonance energy transfer that enables riboflavin trafficking and subcellular localization studies. Mol Pharm. 2004;1:257–66.
33. Apodaca G, Katz LA, Mostov KE. Receptor-mediated transcytosis of IgA in MDCK cells is *via* apical recycling endosomes. J Cell Biol. 1994;125:67–86.
34. Demarre A, Soyez H, Schacht E, Shoaibi MA, Seymour LW, Rihova B. Synthesis and evaluation of macromolecular prodrugs of Mitomycin-C. J Control Release. 1995;36:87–97.
35. Pan SS, Iracki T, Bachur NR. DNA alkylation by enzyme-activated mitomycin C. Mol Pharmacol. 1986;29:622–8.
36. D'Souza VM, Bareford LM, Ray A, Swaan PW. Cytoskeletal scaffolds regulate riboflavin endocytosis and recycling in placental trophoblasts. J Nutr Biochem. 2006;17:821–9.
37. Foraker AB, Ray A, Da Silva TC, Bareford LM, Hillgren KM, Schmittgen TD, *et al.* Dynamin 2 regulates riboflavin endocytosis in human placental trophoblasts. Mol Pharmacol. 2007;72:553–62.
38. Guoand W, Lee RL. Receptor-targeted gene delivery *via* folate-conjugated polyethylenimine. AAPS Pharm Sci. 1999;1:E19.
39. Rachmilewitz B, Sulkes A, Rachmilewitz M, Fuks Z. Serum transcobalamin II levels in breast carcinoma patients. Isr J Med Sci. 1981;17:874–8.
40. Auvinen P, Tammi R, Parkkinen J, Tammi M, Agren U, Johansson R, *et al.* Hyaluronan in peritumoral stroma and malignant cells associates with breast cancer spreading and predicts survival. Am J Pathol. 2000;156:529–36.
41. Nichifor M, Schacht EH, Seymour LW. Macromolecular prodrugs of 5-fluorouracil .2. Enzymatic degradation. J Control Release. 1996;39:79–92.
42. Hoste K, De Winne K, Schacht E. Polymeric prodrugs. Int J Pharm. 2004;277:119–31.
43. Winski SL, Swann E, Hargreaves RH, Dehn DL, Butler J, Moody CJ, *et al.* Relationship between NAD(P)H:quinone oxidoreductase 1 (NQO1) levels in a series of stably transfected cell lines and susceptibility to antitumor quinones. Biochem Pharmacol. 2001;61:1509–16.
44. Cheung RY, Rauth AM, Ronaldson PT, Bendayan R, Wu XY. *In vitro* toxicity to breast cancer cells of microsphere-delivered mitomycin C and its combination with doxorubicin. Eur J Pharm Biopharm. 2006;62:321–31.
45. Chen R, Yue Z, Eccleston ME, Williams S, Slater NK. Modulation of cell membrane disruption by pH-responsive pseudo-peptides through grafting with hydrophilic side chains. J Control Release. 2005;108:63–72.
46. Mukherjee S, Ghosh RN, Maxfield FR. Endocytosis. Physiol Rev. 1997;77:759–803.

47. Maalmi M, Strieder W, Varma A. Ligand diffusion and receptor mediated internalization: Michaelis-Menten kinetics. Chem Eng Sci. 2001;56:5609–16.
48. King AC, Hernaez-Davis L, Cuatrecasas P. Lysomotropic amines cause intracellular accumulation of receptors for epidermal growth factor. Proc Natl Acad Sci U S A. 1980;77:3283–7.
49. Watts PL, Plumb JA, Courtney JM, Scott R. Sensitivity of cell lines to mitomycin C. Br J Urol. 1996;77:363–6.
50. Mahoney BP, Raghunand N, Baggett B, Gillies RJ. Tumor acidity, ion trapping and chemotherapeutics. I. Acid pH affects the distribution of chemotherapeutic agents *in vitro*. Biochem Pharmacol. 2003;66:1207–18.
51. Nomura T, Saikawa A, Morita S, Sakaeda Kakutani T, Yamashita F, Honda K, *et al.* Pharmacokinetic characteristics and therapeutic effects of mitomycin C-dextran conjugates after intratumoural injection. J Control Release. 1998;52:239–52.
52. David A, Kopeckova P, Minko T, Rubinstein A, Kopecek J. Design of a multivalent galactoside ligand for selective targeting of HPMA copolymer-doxorubicin conjugates to human colon cancer cells. Eur J Cancer. 2004;40:148–57.